

Mucoadhesive Itraconazole Nanocrystals With Precise Control of Surface Charge Incorporated to Chitosan Films for Buccal Drug Delivery

Chunyang Zhang, Lucia Lopez-Vidal, Jiawen Wang, Achmad Himawan, Ryan F. Donnelly, and Alejandro J. Paredes*

Drug delivery to mucosal tissues presents considerable challenges related to the complex nature of the mucus layer protecting such tissues. This aggravates when delivering hydrophobic drugs, often requiring incorporation of drugs to nanoparticles and use of mucoadhesive systems. This paper aimed to develop an antifungal chitosan (CHI)-based film loading itraconazole (ITZ) nanocrystals (NCs) with precisely controlled surface charge for enhanced mucoadhesion. Cationic and anionic ITZ NCs are prepared using wet media milling with mean particle sizes and zeta potentials of 226.9 ± 1.4 nm and 234.0 ± 2.90 nm, and $+15.4 \pm 2.8$ mV and -16.2 ± 1.3 mV, for the cationic and anionic NCs, respectively. Cationic ITZ-NCs exhibits a higher affinity to mucin particles. NCs-loaded films showed stronger mechanical properties and adhesiveness compared with ITZ powder-loaded films. Physicochemical analysis reveals that crystalline properties of the ITZ are preserved, with no drug-excipients interaction. A significantly higher amount of ITZ mucosal deposition is obtained from films containing NCs (1360.23 ± 718.73 $\mu\text{g cm}^{-2}$) compared with that from films containing ITZ powder (58.83 ± 37.45 $\mu\text{g cm}^{-2}$). This work demonstrates the feasibility of tailoring the NCs surface, with the resultant systems showing potential for the management of fungal infections in mucosal tissues.

This drug delivery system enables prolonging the residence time of the dosage form at the site of application or absorption.^[1] The binding ability between the polymer and mucosa facilitates the intimate contact of the active pharmaceutical ingredient with the absorption surface, thus enhancing the therapeutic performance of the drug.^[1] Currently, numerous mucoadhesive drug delivery systems have been developed for oral, buccal nasal and vaginal administration for both local and systemic application.

Buccal polymeric films consist of active compounds embedded in polymeric matrix that can be applied to buccal mucosa as drug releasing platform. Biocompatible and biodegradable mucoadhesive films and patches are preferred dosage forms for buccal administration because of flexibility, comfort, lightness, acceptability, capacity to withstand mechanical stress, and customized size.^[2] In addition, the application of films to oral cavity could protect wound surface, thus reducing pain and treating the disease more effectively.^[1] The primary challenges in buccal formulations include

salivary renovation cycle and mechanical stress caused by mastication when drinking or eating.^[3] This could result in the displacement of the films from the application site, reducing contact time and potentially affecting drug absorption. To circumvent this issue, it is necessary to enhance the interaction between drug and membrane barrier of buccal tissue. Therefore, buccal film formulations should be designed to improve the drug permeation across the mucosa to systemic circulation or into submucosal epithelial layers unaffected by the impact of salivary flow, pH, electrolytes, and mucosal enzymes.^[4] One of the most frequently utilised polymers, chitosan (CHI), has been extensively investigated for formulating mucoadhesive buccal films due to its unique physicochemical properties. This biocompatible and biodegradable polymer is positively charged in nature, and it is capable of interacting with the negatively charged O-linked oligosaccharide chains of mucin.^[5] Another important bioactivity of CHI is that it enhances the paracellular transport of active molecules, which contributes to increasing the permeability of the payload of interest across the epithelial barrier.^[6–9] In

1. Introduction

Since the early 1980s, mucoadhesive drug delivery has gained extensive attraction due to its unique physicochemical properties.

C. Zhang, L. Lopez-Vidal, J. Wang, A. Himawan, R. F. Donnelly, A. J. Paredes

School of Pharmacy, Queen's University Belfast
 Medical Biology Centre
 97 Lisburn Road, Belfast BT9 7BL, UK
 E-mail: a.paredes@qub.ac.uk

A. Himawan
 Department of Pharmaceutical Science and Technology
 Faculty of Pharmacy
 Universitas Hasanuddin
 Makassar 90245, Indonesia

© 2024 The Author(s). Advanced Therapeutics published by Wiley-VCH GmbH. This is an open access article under the terms of the [Creative Commons Attribution](https://creativecommons.org/licenses/by/4.0/) License, which permits use, distribution and reproduction in any medium, provided the original work is properly cited.

DOI: 10.1002/adtp.202400209

addition, CHI has antimicrobial activity and the ability to promote wound healing.^[5]

Itraconazole (ITZ) is a potent triazole antifungal agent for the treatment of superficial fungal infections, such as oral and vagina mucosa.^[10] However, the poor solubility of ITZ makes it difficult to formulate in bioadhesive drug delivery system, which results in insufficient bioavailability and reduced therapeutic efficacy. Decreasing particle size is an efficient way to improve the dissolution rate of poorly soluble compounds.^[11,12] Recent developments in nanotechnology have promoted the incorporation of nanocrystals (NCs) in dosage forms for buccal drug delivery.^[13] This aims at reducing the drug particle size to sub-micron range, enhancing dissolution rate of poorly soluble drugs through increased surface to volume ratio.^[13,14] Wet media milling is a technique using top-down mechanism to produce nanosuspensions of crystalline drug particles. Using this technique, the drug powder, dispersed in aqueous stabilizers, is ground by shear forces and collisions, resulting in particles with a mean diameter in the nanometer range (100–1000 nm).^[15] Furthermore, NCs possess a high drug loading (>90%), improving drug absorption on the application site when compared to conventional lipid and polymer nanoparticles.^[13,16] Currently, one of the most noticeable strategies used to enhance the drug permeability via buccal delivery is the application of nanoparticle-based drug formulations.^[13] Both particle size and surface charges of nanoparticles play crucial roles in drug permeability. Roblegg et al. revealed that an increased particle size was attributed to the generation of protein-corona and agglomeration phenomena occurring during the interaction with buccal mucus.^[17] The threshold particle size which facilitated drug permeation across the mucosa was ≈ 200 nm.^[17] Importantly, particles with positive charges exhibited a favorable drug permeation across the porcine buccal mucosa in comparison to those with negative charges, resulting in an improvement in drug penetration and entrapment efficiency.^[17] In addition, the electrostatic interactions between cationic particles and mucus layer could promote the drug release by the replacement of mucin on the particle surface.^[18] Moreover, it has been found that the functional groups on the surface of the nanoparticles can interact with buccal mucosa to form hydrogen bonds, thereby, enhancing the mucoadhesive properties of the formulation.^[19,20] The challenge associated with fabricating NCs-based films is to achieve both homogeneous and mechanically performant films.^[21] The potential of large aggregations and inhomogeneous drug distributions could affect mechanical and mucoadhesive properties of the films. Therefore, reducing particle size to nanoscale could effectively circumvent those limitations.^[22,23] In this study, the poorly soluble drug ITZ was formulated in NCs with a positive surface charge using a wet media milling technique. The mucoadhesive polymer CHI was used as polymeric matrix to formulate oral thin films containing cationic NCs for potential treatment of *C. albicans* via buccal delivery.

2. Experimental Section

2.1. Materials

Poly(vinyl alcohol) (PVA) with a molecular weight of 9–10 kDa and poly(vinylpyrrolidone) (PVP) with a molecular weight of 58 kDa were purchased from Sigma Aldrich, Steinheim, Polox-

amer 407 (P407) was purchased from BASF SE, Ludwigshafen, Germany. CHI with a molecular weight of 10 kDa was purchased from VWR International Ltd, Leicestershire, UK. D- α -tocopheryl polyethylene glycol succinate (TPGS) was purchased from Sigma-Aldrich, Dorset, UK. Sodium dodecyl sulfate (SDS) was purchased from Sigma-Aldrich, Dorset, UK. Polydimethylsiloxane (PDMS) was purchased from Dow Corning Wiesbaden, Germany. Porcine stomach mucin was purchased from Sigma-Aldrich, Dorset, UK. Bidistilled glycerol was purchased from VWR International, Leicestershire, UK. ITZ (purity, $\geq 98\%$) was purchased from Tokyo Chemical Industry, Tokyo, Japan. Zirconia beads partially stabilized with yttria (type YTZP) with a diameter of 0.1–0.2 mm were obtained from Chemco, Guanfu, China. All reagents used in this work were of analytical grade.

2.2. Fabrication and Rationalization of ITZ Nanocrystals

The ITZ NCs were fabricated by wet media milling in a laboratory scale as described previously (Figure 1).^[24] Zirconia beads partially stabilized with yttria (type YTZP) with the diameter of 0.1–0.2 mm were used as milling media. In brief, 100 mg of ITZ powder, 5 mL of stabilizer and 4 mL of zirconia beads were added into a 10.5 mL glass vial. Two magnetic bars (12×6 mm) were added to generate the movement of the whole system. The vial was then closed and fixed on the center of the IKA RCT Basic Magnetic Stirrer (IKA, Staufen, Germany). The system was agitated for 24 h at 1500 rpm at room temperature. The NCs were then separated from the milling beads and magnetic bars using a stainless-steel funnel and sieve with an opening of 38 μ m. During the milling process, the zeta potential of NCs were controlled by applying various types of stabilizers. Cationic ITZ NCs were produced by using a stabilizer combination consisting of a 0.25% w/v CHI solution and 0.5% w/v TPGS. On the other hand, anionic ITZ NCs were prepared using a stabilizer combination comprising 0.05% w/v SDS and 0.7% w/v P407. The particle size and polydispersity index (PDI) of the NCs were rationalized according to the milling time (2, 4, 20, 24 h), size of the milling media (0.1–0.2, 0.4–0.6, 1–2 mm) and drug loading (50, 100, 150 mg).

2.3. Short-Term Stability Study

The stability of the samples obtained from the milling process was studied in terms of their particle size and PDI using dynamic light scattering as detailed in the following section. For this purpose, the aqueous NCs (cationic and anionic) were divided into two parts, one was stored at 25 °C and the other at 4 °C. Both were placed in 2 mL Eppendorf tubes either on the benchtop or in the refrigerator. Samples were taken at predetermined time-points for 21 days, when they were also visually inspected for potential changes such as sedimentation or phase separation.

2.4. Characterization of ITZ NCs

2.4.1. Determination of Particle Size, PDI, and Zeta Potential

At the determined time points, an aliquot of 10 μ L sample was withdrawn from the vial and dispersed in the plastic disposal

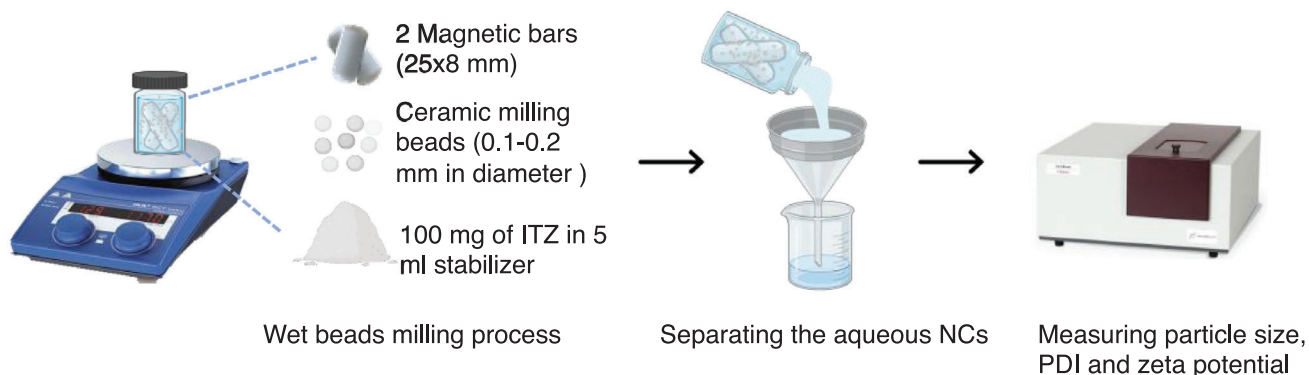


Figure 1. Schematic presentation of ITZ NCs preparation process.

cuvette containing 3 mL deionized water. A NanoBrook Omni analyzer (Brookhaven, New York, USA) was used to measure the particle size and PDI of NCs via dynamic light scattering (DLS). Zeta potential was determined by electrophoretic mobility at the same time. Each sample was measured in three replications at 25 °C.

2.4.2. Mucoadhesion of ITZ NCs

To evaluate the mucoadhesion of the ITZ NCs, the interaction between mucin nanoparticles and ITZ NCs was evaluated based on method from Takeuchi H et al, with modifications.^[25] In the study, the 0.5 w/v mucin solution was prepared in 10 mM buffer (pH = 6.4) and incubated for 4 h at 37 °C with continuous stirring. Then, original mucin nanoparticles (5 mL) were produced by applying a probe sonication (QS4 system, NanoLab, Waltham, MA, USA) at 40% amplification (20 s on, 10 s off for 5 cycles). The mucin suspensions were centrifuged using Eppendorf® 5804 series centrifuge (Eppendorf UK Ltd., Stevenage, UK) at 3500 rpm for 5 mins to obtain fine mucin nanoparticles from the supernatant. Afterwards, the nano sized mucin particles (3 mL) were separately incubated with 1 mL cationic or anionic ITZ NCs sus-

pensions (200 times diluted in deionized water) at 37 °C oven for 2 h. Additionally, fine mucin nanoparticles (3 mL), 200 times diluted cationic ITZ NCs suspensions (3 mL) and anionic ITZ NCs suspensions (3 mL) were also individually incubated at the same conditions for comparison. The particle size, PDI and zeta potential of the fine mucin particles, cationic ITZ NCs, anionic ITZ NCs and mucin nanoparticles/ITZ NCs mixtures were measured before and after incubation.

2.5. Preparation of ITZ-Loaded Films

The ITZ-loaded films were prepared using a solution casting methodology (Figure 2). First, the master mold was designed with ThinkerCAD software (AutoDesk, San Rafael, California) and prepared using a 3D printer (Anycubic Photon S) and Anycubic UV sensitive resin. Afterwards, the mold for preparation of films with dimensions of 20 mm x 20 mm x 2 mm was reverse-molded from the master mold using PDMS.

CHI was used as a biopolymeric excipient to formulate ITZ-containing thin films owing to its excellent film-forming ability and mucoadhesive property. Low molecular weight CHI was selected because it has better biodegradability, biocompatibility, and

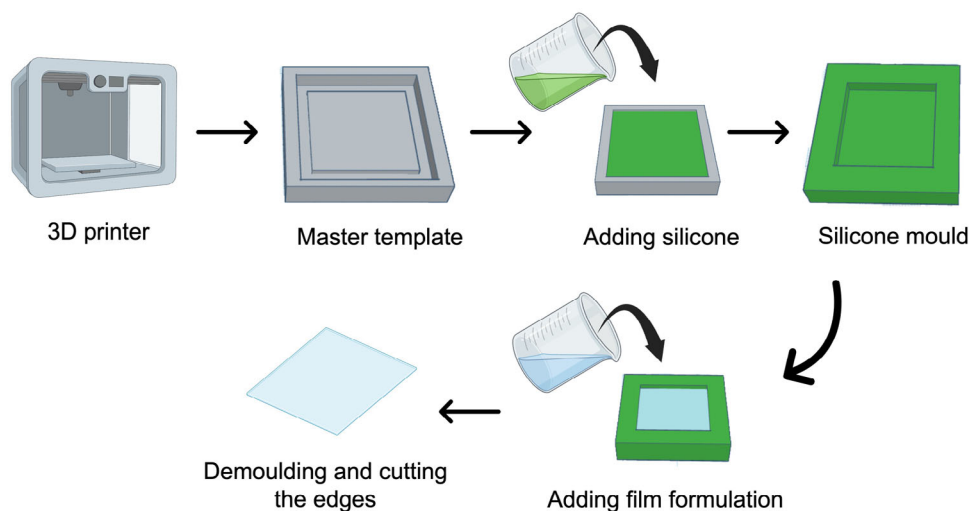


Figure 2. Schematic presentation of the ITZ-loaded films.

bioactivity as well as lower toxicity compared to high molecular weight CHI.^[26] Prior to casting the ITZ-loaded films, the film matrix was prepared by dissolving 1 g of CHI powder in 50 mL of 1% w/v acetic acid. The aqueous film formulations were then prepared by blending 2% w/v CHI solution and ITZ NCs at different volume ratios (1:1, 1:2, 1:3, and 1:4). An aliquot of 1 mL of mixture was transferred into the mold and placed in the fume hood overnight for drying and evaporation of acetic acid. Similarly, the physical mixture (PM) films containing coarse ITZ powder and stabilizers were also fabricated by physically mixing the 2% w/v CHI solution with all the components in ITZ NCs as the protocol mentioned above. Each film formulation contained 30 mg of glycerol as a plasticizer. After drying, the films were gently peeled off from the molds and wrapped in the aluminum for the following characterizations.

2.6. Characterization of ITZ-Loaded Films

2.6.1. Morphology of the ITZ-Loaded Films

The morphology of the films was observed using a tabletop scanning electron microscope (SEM) (Hitachi, Tokyo, Japan) and optical coherence tomography (OCT) (EX1301 VivoSight, Michelson Diagnostics Ltd., Kent, UK).

2.6.2. Measurement of Thickness and Folding Endurance of the ITZ-Loaded Films

Due to the formation of side walls during the film drying, sections of the film with the most homogeneous drug distribution were selected for the following measurements. The side walls were carefully removed using a scalpel before the following measurements. A digital vernier caliper was used to measure the thickness of each film. Folding endurance values were determined by repeatedly folding each film 300 times at the same location, or until it broke. All the measurements were performed in three replications.

2.6.3. Thermal Analysis

The aqueous ITZ NCs suspension was lyophilized into NCs powder prior to thermal analysis. The details of the lyophilization cycle were presented in Section S1 (Supporting Information) Thermal analysis was performed using a Q100 differential scanning calorimetry (DSC) (TA Instruments, Surrey, UK) and Q500 thermogravimetric analysis (TGA) (TA Instruments, Surrey, UK) to determine the physical state of the ITZ, lyophilized NCs, ITZ-loaded films and base materials of the film formulation. In DSC study, samples with a weight of 5–10 mg were placed and sealed in a standard aluminum pan. An empty aluminum pan was utilized as a reference. The running was carried out under a temperature-programmed conditions with a range from 25 to 300 °C. The heating rate was controlled at 10 °C min⁻¹ under nitrogen flow. Similarly, TGA study was conducted between 25 °C and 500 °C with a heating rate of 10 °C min⁻¹ under a nitrogen flow.

2.6.4. Attenuated Total Reflectance Fourier Transform Infrared

The attenuated total reflectance Fourier transform infrared (Accutrac FT/IR-4100 Series, Jasco, Essex, UK) was applied to evaluate the potential physical and chemical interactions of the drug-excipient between the ITZ and base formulation materials. In this study, the samples were clamped between the stage of the sample holder and a digital torque controller. The range of the scanning varied from 4000 to 600 cm⁻¹ with a resolution of 4 cm⁻¹.

2.6.5. Powder X-Ray Diffraction

To determine the crystallographic structure, powder X-ray diffraction (XRD) patterns of the ITZ, lyophilized ITZ NCs and physical mixture were obtained and analyzed using a powder X-ray diffractometer (Bruker D8 Discover, Bruker Corporation, California, America). Copper K- α was used as X-ray energy in this equipment. Before measurement, each sample was placed into a sample holder with a 1 mm depression. The sample was irradiated with a beam of X-rays and scanned within a 2θ range of 0–60° in continuous mode. The scanning speed was 2° per minute.

2.6.6. Mucoadhesion Study of the ITZ-Loaded Films

The mucoadhesion study of the films was performed using a TA.XT.Plus Texture Analyser (Stable Microsystems, Surrey, England) as described by Andrews et al.^[27] For this purpose, a mucin disc was prepared by mixing 90% w/w porcine mucin powder and 10% w/w microcrystalline cellulose (MCC) using dual asymmetric centrifugation at 2500 rpm for 3 min (Hauschild Speed-Mixer, Waterkamp, Germany). Subsequently, 250 mg of mixture was compressed with a force of 10 tons for 30 s to obtain the mucin discs with the diameter of 13 mm. MCC powder was added during the compression to prevent the discs from being broken. Then, the mucin disc was attached on the aluminum block using cyanoacrylate glue. The attached mucin disc was hydrated by adding 50 μ L of mucin solution (5% w/v), followed by removing the excessive solution from the surface of the disc. After that, ITZ-loaded film was attached on the movable cylindrical Texture Analyzer probe using double-side adhesive tape. The probe was programmed moving down to contact the mucin disc with a force of 1 N for 30s. The force required to detach the film from the mucin disc was recorded and defined as the mucoadhesive strength.

2.6.7. Tensile Strength of the ITZ-Loaded Films

The tensile mechanical properties of the ITZ-loaded films were tested using a TA.XT.Plus Texture Analyzer with an extension speed of 10.2 mm min⁻¹. Prior to the study, the ITZ NCs-loaded and ITZ powder-loaded films were prepared using PDMS mold with dimensions of 40 mm x 60 mm x 2 mm, followed by cutting into strips with the width of 0.5 mm. Two ends of the strips were clamped with an inter-clamp distance of 40 mm. The thickness of the stripes was measured using a digital vernier caliper to

calculate the cross-sectional area. The percentage of the elongation was directly recorded by the equipment when the strip was broken. The measurement was carried out in three replicates.

2.6.8. Drug Loading of the ITZ-Loaded Films

Drug loading was determined from the films loaded with ITZ NCs and coarse ITZ. Briefly, film discs in diameter of 8 mm were obtained from the central part of the whole film using a biopsy punch. Then, film discs were dissolved in 5 mL of 1% w/v acetate acid and sonicated in a water bath until completely dissolved. Afterward, an aliquot of 100 μ L suspensions was transferred into a 2 mL Eppendorf tube containing 1900 μ L acetonitrile. Then, the samples were centrifuged using a Sigma benchtop microcentrifuge (SciQuip Ltd, Shropshire, England) at 16162 x g for 20 mins, and the supernatant was diluted 10 times with mobile phase before HPLC analysis.

2.6.9. In Vitro Drug Release of the ITZ-Loaded Films

The in vitro drug release study was carried out by placing either ITZ NCs-loaded films or ITZ powder-loaded films into falcon tubes containing 40 mL of release medium. To achieve sink conditions, various release mediums, including PBS (pH = 7.4), 1% w/v SDS in PBS, 0.1 mol L⁻¹ hydrochloric acid (HCl) and 1% w/v SDS in 0.1 mol L⁻¹ HCl were evaluated based on the solubility of the drug. The release medium with the highest saturated solubility was selected for in vitro drug release. The films containing equivalent to 2.6 mg of pure drug were transferred into the release medium, which was placed in a 37 °C incubator at 40 rpm. At determined time points, an aliquot of 1 mL of samples was withdrawn and replaced with fresh release medium. The samples were then centrifuged using Sigma 1–14 bench-top microcentrifuge (SciQuip Ltd, Shropshire, England) at 16 62 x g for 20 mins to remove the suspended ITZ NCs prior to HPLC analysis using the method described in section 2.6.11.

2.6.10. Buccal Mucosal Deposition of the ITZ-Loaded Films

The ex vivo buccal mucosal deposition study was performed according to the method described previously, with modifications.^[28] The buccal mucosa was obtained from still-born piglets and excised within 24 h of birth using a sterilized scalpel. The excised mucosa was stored in a -20 °C freezer until use. Before the study, the neonatal porcine oral mucosa was defrosted at room temperature and activated using pH 6.4 mucus buffer. The mucosa was then gently wiped using tissue paper to remove excessive buffer. Each excised mucosa was placed in a weighting boat containing PBS-soaked tissue paper. After that, a 3D-printed resin ring with an inner diameter of 6 mm and height of 5 mm was attached using cyanoacrylate glue. The films containing NCs and PM were cut into discs in a diameter of 5 mm to fit the 3D printed rings. Inside the ring, three NCs-loaded discs were stacked on the mucosa surface. For the control group, the same procedure was followed, using two PM-loaded discs stacked on top each other to match the drug

content from NCs group. An aliquot of 10 μ L of buffer (pH = 6.4) was added to mimic the pH value of the buccal environment. The whole weighing boat was sealed properly using Parafilm M and incubated in a 37 °C oven for 24 h. At the end of the study, the resin rings and residual formulation were removed, followed by washing the mucosa using 3 mL of PBS. Afterwards, a biopsy punch with a diameter of 8 mm was applied to obtain the section of the mucosa where the films were applied. The mucosal sections and 2 stainless steel beads (0.5 cm diameter, Qiagen, Hilden, Germany) were then placed in 2 mL Eppendorf tubes containing 0.5 mL acetonitrile. Mucosa samples were disrupted in a Tissue Lyser (Qiagen, Ltd, Manchester, UK) for 10 min at 50 Hz. The samples were subsequently centrifuged for 20 min at 16162 x g (SciQuip Ltd, Shropshire, England) prior to quantification with the validated HPLC method described in the following section.

To visualize the distribution of penetrated NCs in the oral mucosa, Nile Red (NR) was selected as a model drug for the fabrication of NCs. The NR-loaded films were also cast for mucosal deposition. The same protocols were utilized for the preparation of NR NCs and NR-loaded films. NR NCs-loaded film and NR powder-loaded films were separately applied on the oral mucosa as mentioned above. At the end of the study, the buccal mucosa was cleaned properly and embedded in optimal cutting temperature compound before freezing in liquid nitrogen (-80 °C). A cryostat microtome (CM 1900-1-1, Leica, Nussloch, Germany) was applied to section the tissue into microscopic slices from cross-sections with a thickness of 10 μ m. The slices were observed under a digital microscope.

2.6.11. Instrumentation and Chromatographic Conditions for Analytical Method

For in vitro and ex vivo studies, ITZ was quantified using reverse phase HPLC equipped with UV detector (Agilent Technologies 1200 Infinity UK Ltd, Stockport, UK) and an Inertsil (ODS3) C-18 column (250 mm x 4.6 mm, 5 μ m) with the flow rate of 1 mL min⁻¹. The UV absorption was fixed at 270 nm, and the injection volume was controlled at 50 μ L. The mobile phase consists of 90% acetonitrile and 10% acetate acid (0.1% w/v). The analysis was performed at room temperature. This analytical method was validated according to the International Council on Harmonization (ICH) Q2 (R1) guidelines.^[29]

2.6.12. Statistical Analysis

GraphPad Prism software (version 10.0, GraphPad Software Inc, San Diego, California, USA) was used to perform statistical analyses. A t-test was applied for comparing two groups, whereas one-way ANOVA was utilized for comparing multiple groups. In all cases, $p < 0.05$ was considered a significant difference.

3. Results and Discussion

3.1. Fabrication and Rationalization of ITZ Nanocrystals

The ITZ NCs were successfully prepared using wet media milling technique at a laboratory scale, which was a top-down

method to create nanosized particles from bulk material by applying high-energy shear or friction force.^[24] During the NCs preparation process, stabilizers provide ionic or steric stability by adhering to the surface of the NCs, thereby preventing the aggregation of the nanoparticles.^[30] Low molecular weight CHI has higher solubility and lower viscosity due to its shorter chains and free amine groups on the glucosamine unit, allowing for broader pharmaceutical applications.^[31] In this study, 10 kDa chitosan was used as a stabilizer to prepare cationic NCs. Critically, low molecular weight polymers lead to a lower slurry viscosity and more bead movement during milling, thus enhancing energy input and improving NCs dispersion in the stabilizer. CHI is a biocompatible and biodegradable polymer with cations that has been widely used fabrication of NCs. Abbate et al. successfully developed antiretroviral drug NCs stabilized using the combination of CHI and TPGS solution.^[32] CHI also exhibits mucoadhesive properties, enabling CHI nanoparticles to be administered via transmucosal routes, such as intranasal, intraocular, intravaginal, intratracheal, intrapulmonary, and other routes.^[33] Nanoparticles prepared with CHI and CHI derivatives typically possess positive surface charges and mucoadhesive properties, which enables them to adhere to mucus membranes and release the drug payload in a sustained release manner.^[10] CHI mucoadhesion can locally increase the concentration of a drug and thus increase the driving force for drug diffusion into cells, which could be advantageous even if the nanoparticles themselves remain trapped extracellularly in mucus. SDS is a commonly used anionic surfactant for preparation of NCs. The stabilizer combination of SDS and P407 was used to prepare ITZ NCs has also been reported.^[34] ITZ NCs were rationalized based on the milling time, size of milling media and drug loading. For both ITZ NCs formulations, the particle size and PDI decreased after 24 h of milling (Figure 3A,D). The particles size of cationic and anionic NCs were 226.92 ± 1.40 nm and 149.05 ± 0.63 nm, respectively. In order to obtain similar particle sizes between cationic and anionic NCs, the milling time for anionic NCs was controlled at 4 h, resulting in a particle size of 234.00 ± 2.90 nm. Additionally, size of the milling media had an effect on the particle size and PDI. As shown in Figure 3B,E, milling beads with a diameter of 0.1–0.2 mm produced ITZ NCs with a PDI value below 0.2. Figure 3C,F revealed that the drug loading of 100 mg led to favorable particle size and narrow size distribution for both ITZ NCs formulations. In this bead-milling system, the NCs were generated via attrition and collision forces generated by grinding beads. Typically, smaller milling beads produced small NCs, resulting from the increased chances of collisions between coarse drug particles and milling media.^[35,36] Moreover, longer grinding time led to smaller particle size and narrow size distributions. However, in most milling experiments, it was observed that a plateau of size reduction was achieved after a certain milling duration.^[37]

3.2. Short-Term Physical Stability

A challenge associated with NCs in suspension is their tendency to aggregate and undergo crystal growth due to Ostwald ripening.^[38] Consequently, it is important to assess the physical stability of these nanoparticles. To address this, the particle size

and PDI of the obtained ITZ NCs were monitored over 21 days, as shown in Figure 4. The particle size and PDI of the ITZ NCs, both cationic and anionic, remained within relatively unchanged throughout the evaluation period, demonstrating the system's ability to maintain NCs stabilization without significant changes. As depicted in Figure 4A, the particle size of the cationic ITZ NCs increased slightly more under ambient conditions (25 °C), although the difference was only 30 nm over the 21 days studied. However, the differences were not statistically significant ($p < 0.05$). Additionally, a visual inspection of the suspension at the end of the study showed no signs of precipitation or phase separation, with no appreciable visual differences compared to day 0 (Figure 4E,F, respectively).

3.3. Characterization of ITZ NCs

3.3.1. Determination of Particle Size, PDI, and Zeta Potential

The average particle size and PDI of the final ITZ NCs formulations were determined using DLS. As shown in Figure 3G, the DLS graph demonstrated that both types of ITZ NCs had monomodal size distributions with PDI values of 0.17 and 0.16, respectively. The zeta potentials were used to evaluate the surface charge of the NCs in solution, which were determined by the electrochemical equilibrium at the particle-liquid interface.^[39] Zeta potential is a key physical property of NCs, providing the information of potential stability of NCs in suspension system. If the absolute zeta potential of NCs is low, aggregation of NCs in suspensions occurs due to gravitational attraction between the individual particles exceeding the electrostatic repulsion.^[30] Typically, an absolute value of zeta potential above 30 mV is required for electronic stabilization. However, for NCs suspensions that are stabilized by the combination of electrostatic and steric stabilization, a zeta potential $>+20$ mV or $\leftarrow 20$ mV usually provides a high degree of physical stability.^[40] In this study, the zeta potential of rationalized NCs formulations were $+15.43 \pm 2.79$ mV and -16.20 ± 1.30 mV, respectively (Figure 3H). Both ITZ NCs formulations were stabilized by using a combination of electrostatic and steric stabilization. The concentration of steric stabilizers (TPGS and P407) was much higher than ionic stabilizers (CHI and SDS), indicating the drug particle surface was densely covered by the chains of steric stabilizers. Therefore, NCs' surface potential was not dramatically affected by the concentration of ionic stabilizers. The stability of the nanosuspension system was achieved by the synergistic actions of stabilizers with different mechanisms, implying the achievement of an optimal balance between electrostatic repulsion and spatial stability of the NCs.^[30]

3.3.2. Mucoadhesion Study

This study was carried out to evaluate the mucoadhesion properties between ITZ NCs and mucin nanoparticles. The particle size, PDI and zeta potential of the cationic NCs, anionic NCs and mucin nanoparticles remained similar before and after the individual incubation (Figure 5A–C). However, after incubation with mucin nanoparticles, the particle size and PDI of cationic

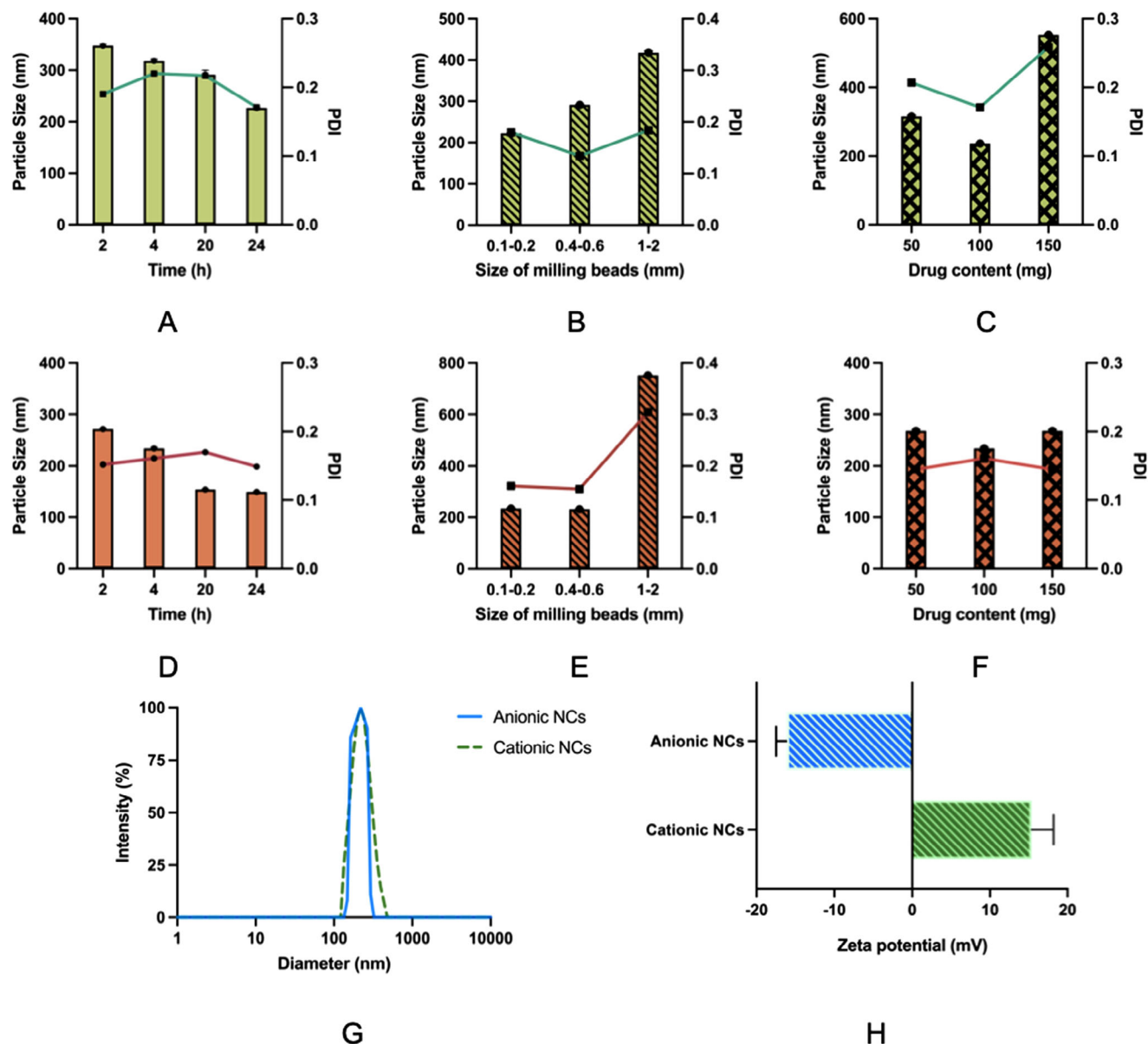


Figure 3. Mean particles size and PDI of cationic ITZ NCs rationalized by applying different milling periods A), sizes of milling media B), drug contents C) (means + S.D., $n = 3$); mean particles size and PDI of anionic ITZ NCs rationalized by applying different milling periods D), sizes of milling media E), drug contents F) (means + S.D., $n = 3$); particle size distribution of both ITZ NCs G); zeta potential of ITZ NCs H) (means + S.D., $n = 3$).

NCs increased to 1013.98 ± 112.88 nm and 0.33 ± 0.03 , respectively. These values were significantly higher than those observed for anionic NCs incubated with mucin nanoparticles ($p < 0.05$) (Figure 5D). The adsorption of CHI molecules onto the negatively charged mucin particles was responsible for these increased values. Previous studies showed that CHI interacts with mucin to form a complex by ionic or hydrogen bonding as well as through hydrophobic interactions.^[10] The increased particle size and PDI could be ascribed to the formation of the aggregates between sub-micro sized mucin particles and positively charged ITZ NCs. The zeta potentials of both mucin/ITZ NCs mixtures decreased after incubation could result from the dilution by introducing mucin nanosuspensions (Figure 5E). The zeta potential of the mucin

and CHI/TPGS NCs mixture decreased to -2.87 ± 1.18 mV compared to the original zeta potential of mucin nanosuspension (-6.30 ± 2.98 mV). This may also be attributed to the neutralization of the positively charged NCs and negatively charged mucin particles. According to the higher mucoadhesive affinity to mucin particles, cationic ITZ NCs were selected for further film casting and characterization.

3.4. Preparation of ITZ-Loaded Films

Different ratios were investigated to cast CHI films containing ITZ in attempt to load a high concentration of ITZ NCs. The

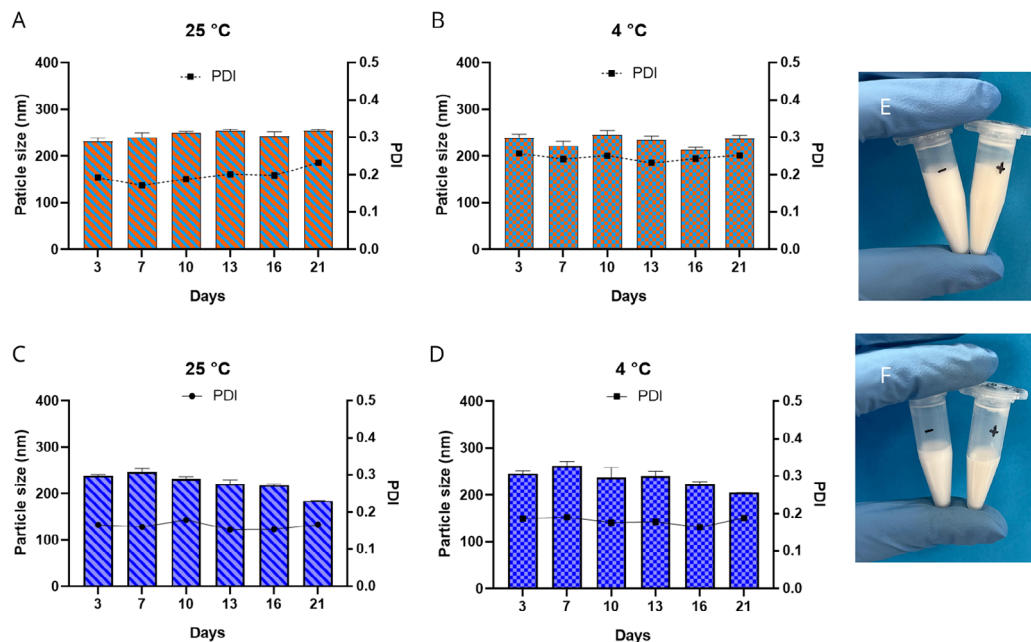


Figure 4. Mean particle size and PDI of cationic ITZ NCs stored at 25 °C A) and 4 °C B) (means + S.D., $n = 3$); mean particle size and PDI of anionic ITZ NCs stored at 25 °C C) and 4 °C D) (means + S.D., $n = 3$). Appearance of the cationic (+) and anionic (-) ITZ NCs on day 0 E) and day 21 F).

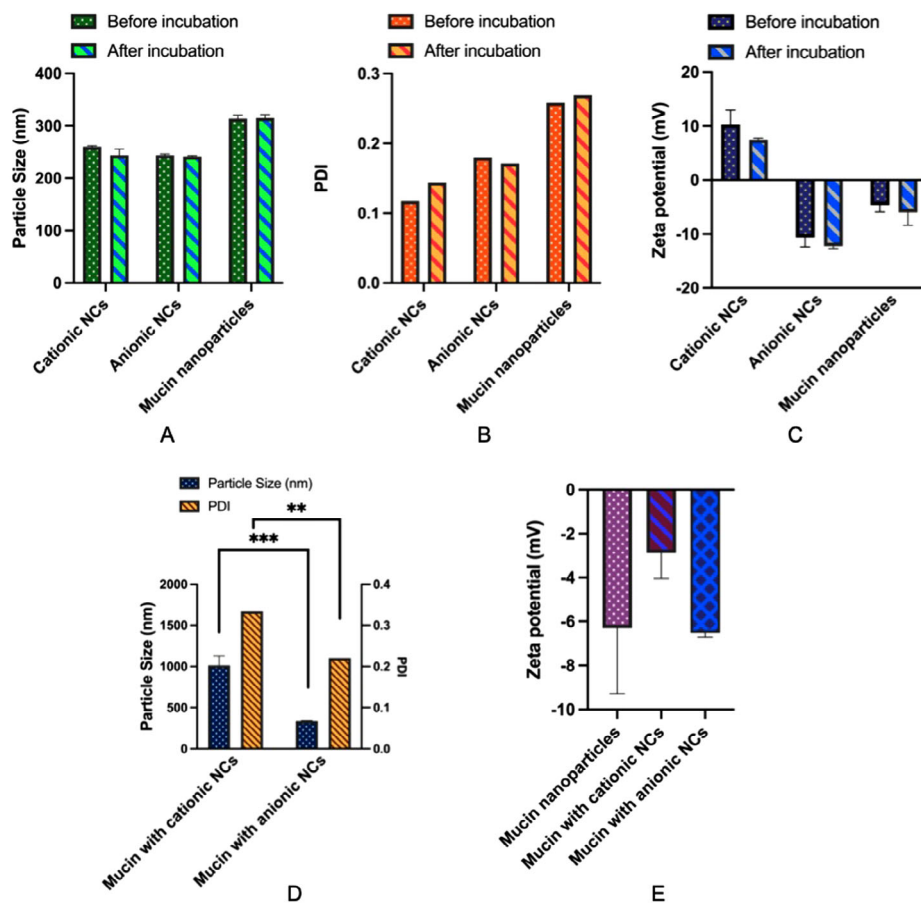
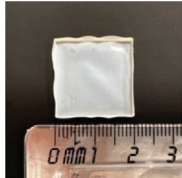
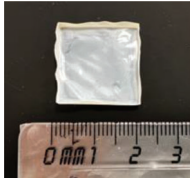
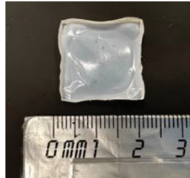



Figure 5. Particle size, PDI and zeta potential of cationic NCs, anionic NCs and mucin nanoparticles before and after individual incubation A–C) (means + S.D., $n = 3$); particle size and PDI of cationic NCs and anionic NCs after incubation with mucin suspensions D) (means + S.D., $n = 3$); zeta potential of cationic NCs and anionic NCs after incubation with mucin nanosuspensions E) (means + S.D., $n = 3$).

Table 1. Formulations investigated for ITZ NCs-loaded films using several ratios.

Formulation code	F1	F2	F3	F4
Ratio of NCs suspensions and CHI solution (v/v)	1:1	2:1	3:1	4:1
Observations	Good film-forming ability 	Good film-forming ability 	Good film-forming ability 	Poor film-forming ability 

film-forming ability and surface morphology were observed by the naked eye. The results in **Table 1** indicates that the films fabricated using a 3:1 ratio of NCs suspensions to CHI polymer exhibited flexible properties and smooth surfaces. However, films prepared using a higher volume ratio were fragile and difficult to demold.

3.5. Characterization of ITZ-Loaded Films

3.5.1. Morphology of the ITZ-Loaded Films

As displayed in **Figure 6A–D**, a smooth surface without any obvious drug particles was observed from NCs-loaded film using a digital microscope (Leica Microsystems, Milton Keynes, UK) and SEM, revealing that a homogeneous drug distribution was achieved via nanosizing the coarse drug into NCs. The cross-sections of both films were obtained using OCT, a non-invasive

optical imaging technique that maps the variation of the reflected light from a sample as a function of depth.^[41] As depicted in **Figure 6E**, the films incorporated ITZ NCs showed a homogeneous thickness compared to films loaded with coarse ITZ (Figure 6F). In contrast with coarse ITZ-loaded films, NCs-loaded films showed an intense and uniform light reflection from the sample surface, which suggests the dense nature of the film and a homogeneous drug distribution. However, a less intense light reflection was observed from films containing coarse drug, which could be explained by the inhomogeneous dispersion of light by the larger coarse drug particles.

3.5.2. Measurement of Thickness and Folding Endurance of ITZ-Loaded Films

The thickness and folding endurance of the films were essential measurements, as they are associated with oral com-

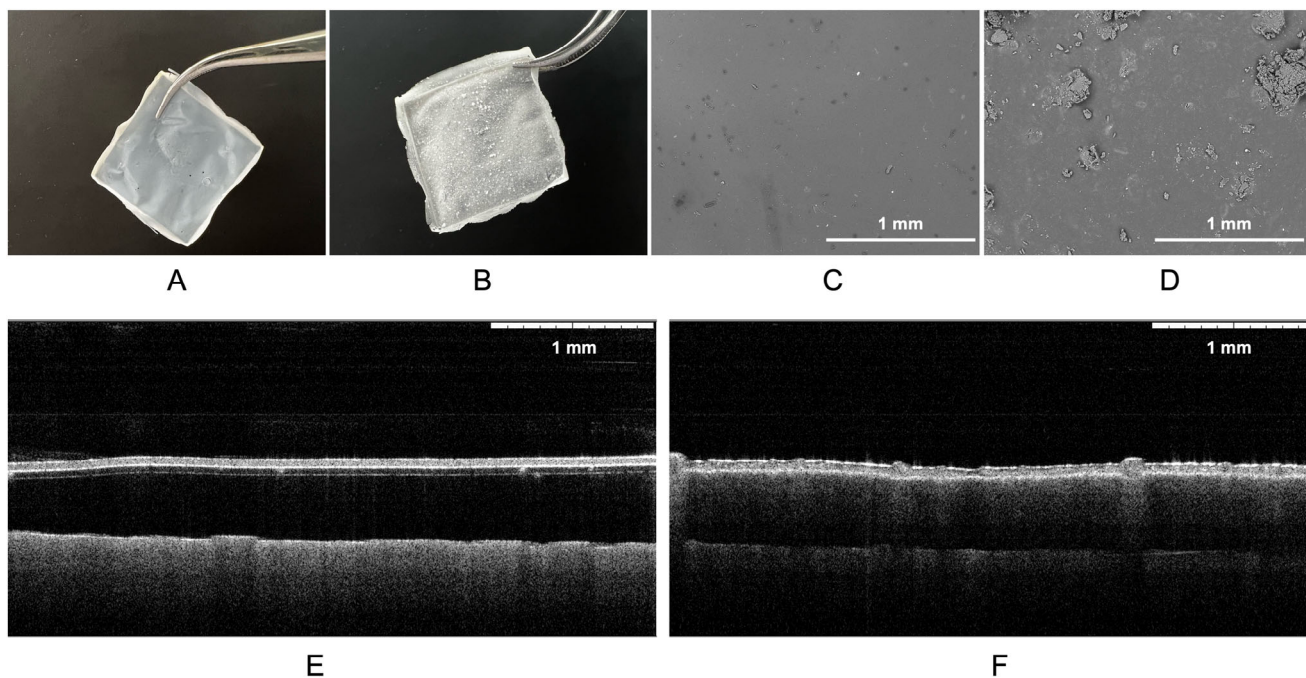


Figure 6. Morphology of films loaded ITZ NCs and coarse ITZ powder observed using digital microscope (A,B); morphology of films loaded ITZ NCs and coarse ITZ powder observed using SEM (C,D); morphology of films loaded ITZ NCs and coarse ITZ powder observed using OCT (E,F).

Table 2. Thickness and folding endurance of ITZ-loaded films.

	Thickness [mm]	Folding endurance [times]
NCS-loaded film	0.04 ± 0.01	More than 300
PM-loaded film	0.06 ± 0.01	More than 300

fort (Table 2). ITZ NCS-loaded films were slightly thinner than coarse ITZ-loaded films, with both films showing a small variation in thickness. This result may be due to the presence of big aggregates, which disrupted the polymeric matrix of the films, preventing an adequate compaction during measurement. The folding endurance in this study evaluated the flexibility of the films so that they could be easily manipulated. In general, folding endurance values of more than 300 were considered an excellent durability and flexibility of the films.^[42]

3.5.3. Thermal Analysis

As shown in Figure 7A, pure ITZ exhibited an intense endothermic peak that appeared at 170 °C, corresponding to the melting point of drug crystals. However, the endothermic peak of the lyophilized ITZ NCS appeared at 159 °C. This shift in peak toward a lower melting point could be attributed to the reduction of drug particle size to nanoscale.^[43] For both ITZ-loaded films, a noticeable shift of the ITZ peaks was observed, likely resulting

from the addition of the amorphous CHI. This indicated that interactions between CHI and the drug molecule may occur, potentially altering the thermal behavior of ITZ. The DSC curve of CHI powder showed a broad endothermic peak near 100 °C, suggesting that CHI typically undergoes dehydration, which involves the loss of water molecules that are hydrogen-bonded to hydrophilic groups.^[44,45] Figure 7B exhibits the TGA curves of ITZ powder, ITZ NCS, ITZ-loaded films and CHI powder. TGA analysis revealed similar decomposition behavior of coarse ITZ powder and lyophilized ITZ NCS, starting around 380 °C. Both ITZ-loaded films presented an initial weight loss from 30 to 80 °C, which could be associated with residual moisture evaporation. The following stepwise weight loss occurred over a wide temperature range, from 130 to 310 °C, and was attributed to the degradation of CHI.^[46]

3.5.4. Attenuated Total Reflectance Fourier Transform Infrared

The FTIR analysis (Figure 7C) revealed that the peaks observed between 3081 cm^{-1} and 2815 cm^{-1} were corresponding to alkane and amine groups.^[47] The multiple characteristic peaks were observed between 1696 cm^{-1} and 1448 cm^{-1} in the spectrum of ITZ powder, which may be attributed to C = C stretching vibrations in aromatic rings. Characteristic peaks in the region of 1350–1275 cm^{-1} were associated with C-N or C-O stretching vibrations. The broad and strong peaks approximately between 3600 cm^{-1} – 2900 cm^{-1} were obtained in ITZ-loaded films and CHI powder

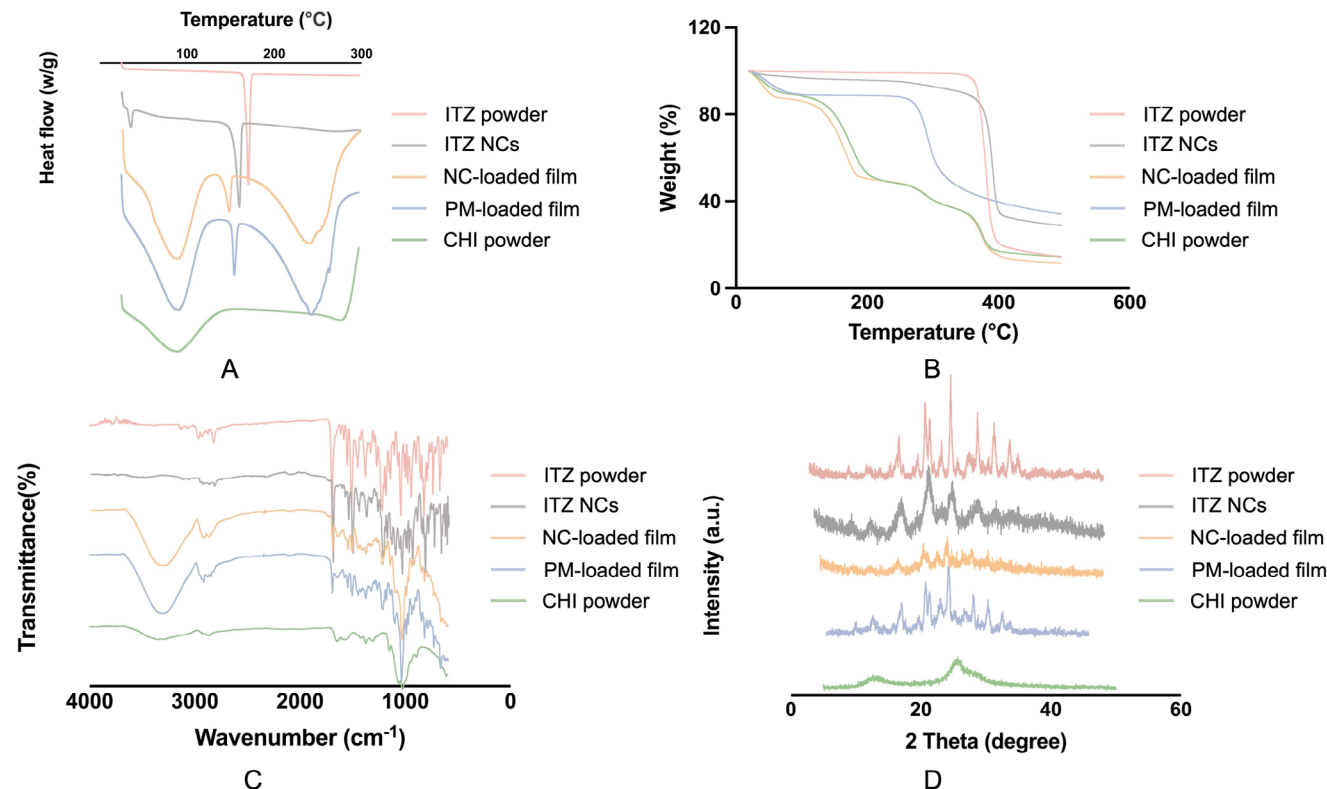


Figure 7. DSC thermograms of the ITZ powder, lyophilized ITZ NCS, ITZ-loaded films and CHI powder A); TGA thermograms of the ITZ powder, lyophilized ITZ NCS, ITZ-loaded films and CHI powder B); ATR-FTIR spectra of the ITZ powder, lyophilized ITZ NCS, ITZ-loaded films and CHI powder C); diffractograms of the ITZ powder, lyophilized ITZ NCS, ITZ-loaded films and CHI powder D).

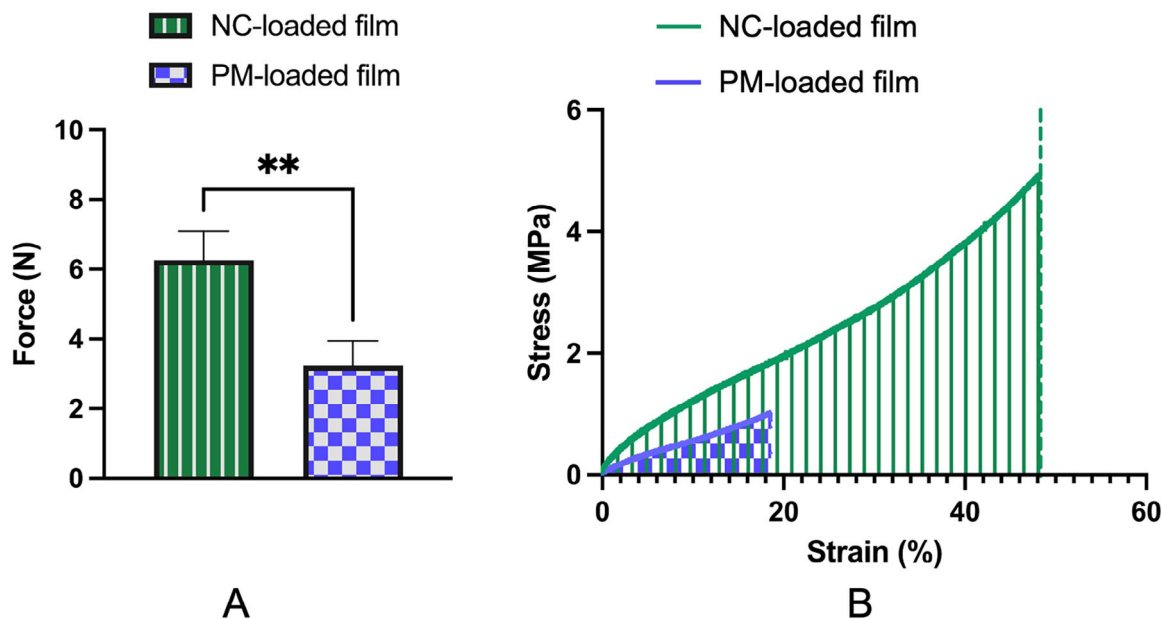


Figure 8. Adhesion force for ITZ-loaded films A) (means + S.D., $n = 3$); Representative stress versus strain curves for ITZ-loaded films B).

due to the presence of the O-H group in CHI. All the characteristic bands of ITZ were found in the lyophilized ITZ NCs, NCs-loaded films and PM-loaded films. However, no additional peaks were observed, indicating the absence of chemical interactions between the pure ITZ and base materials. The original properties of ITZ were preserved during beads milling, film casting and drying process.

3.5.5. Powder X-Ray Diffraction

XRD was applied to evaluate the crystallinity of ITZ-loaded samples. XRD diffractograms of pure ITZ, lyophilized ITZ NCs, ITZ-loaded films and CHI powder are presented in Figure 7D. Crystallinity of the ITZ-loaded samples was investigated by comparing their representative peaks with that of pure ITZ powder, as a reference. The diffractogram of pure ITZ exhibited sharp peaks at angles (2θ) of 18.79°, 22.51°, 22.77°, 23.48°, 25.25°, 26.64°, 30.71°, 33.32°, 35.78°, revealing ITZ was in a high crystalline form. Several characteristic peaks remained in the lyophilized ITZ NCs, NCs-loaded films and PM-loaded films. Although the crystalline state of ITZ was partially preserved during the preparation of NCs, the intensity of peaks was dramatically diminished, probably resulting from the high-speed milling process. In addition, the diffractograms clearly exhibit continuously broad characteristic peaks, which indicate the loss of long-range order in the crystalline material during grinding.^[48] CHI was shown to be amorphous without any sharp peaks.

3.5.6. Adhesion Study of the ITZ-Loaded Films

The adhesion strength was measured as the maximum force required to separate the film from the buccal cavity, which provided insights into film retention on the applied site. However, there

are no standard method to determine this important parameter. In this study, adhesive properties of the CHI-based patches were evaluated using compressed porcine mucin discs and TA-XT Plus Texture Analyzer.^[27,49] As demonstrated in Figure 8A, the patches incorporated with ITZ NCs showed a significantly enhanced adhesion (6.26 ± 0.83 N) compared to patches loaded with PM, which showed a force of 3.22 ± 0.72 N ($p < 0.05$). In addition to the inherent adhesive properties of CHI itself, the improved adhesion may be attributed to the smooth surface of the film containing ITZ NCs, increasing the contact points between both surfaces. The adhesion force of the buccal film is crucial to improve residency, ultimately enhancing clinical performance and patient compliance. However, it is worth noting that the results from in vitro may not correlate well with those from in vivo, as numerous factors (saliva secretion, mastication, and mucus turnover) that can obviously affect the adhesion strength and duration of adhesion, are absent during in vitro studies.^[50]

3.5.7. Tensile Strength of the ITZ-Loaded Films

A tensile mechanical test was performed with the CHI-based films loaded with ITZ NCs and ITZ powder. The representative tensile stress-strain curves are presented in Figure 8B. The tensile strength of CHI films containing ITZ NCs was found to be 4.81 ± 0.34 MPa and the elongation at break $44.70 \pm 2.97\%$. However, the film incorporated with ITZ powder exhibited a higher stiffness with a tensile strength up to 0.89 ± 0.33 MPa and the elongation at break $18.61 \pm 3.21\%$. The difference in flexibility between these two formulations was likely due to the drug distribution in the film. The presence of ITZ coarse particles, inadequately dispersed within the CHI matrix, may act as potential defects in the film. This could lead to the films breaking more easily at these points during elongation, likely due to the uneven force distribution. In addition, NCs could also serve as

Table 3. Saturated solubilities of ITZ in different release mediums for in vitro drug release.

Release medium	Saturated solubility [$\mu\text{g mL}^{-1}$]
PBS (pH = 7.4)	Not detectable
0.1 mol/L HCl	0.88 ± 0.29
1% w/v SDS in PBS (pH = 7.4)	87.72 ± 5.34
1% w/v SDS in 0.1 mol/L HCl	650.37 ± 116.27

physical crosslinking points within CHI networks. Their small particle size and high surface area facilitated the interactions between NCs and CHI molecules via physical interactions, such as hydrogen bonding, electrostatic interactions and van der Waals.^[28,51] The formation of the network structures consequently enhanced the mechanical properties of the CHI-based films.

3.5.8. Drug Loading of the ITZ-Loaded Films

The drug content in the two formulations were $0.90 \pm 0.17 \text{ mg cm}^{-2}$ and $1.23 \pm 0.26 \text{ mg cm}^{-2}$ for NCs-loaded films and PM-loaded films, respectively. The difference in drug loading between formulations could be attributed to surface tension of the aqueous film formulation. Surface tension may cause the aqueous formulation to accumulate towards the edges of the square mold, resulting in the surface of the liquid to form a curve in contact with the inner wall of the container. This effect occurs when the attraction between the particles of the liquid and the container (adhesion) is more than half the attraction of the particles of the liquid to each other (cohesion), causing the liquid to climb the walls of the container.^[52] Crucially, in this study, NCs suspended in CHI gel accumulated at the edge of the mold in a larger extent than ITZ powder, which sedimented at the bottom of the mold due to the gravity, leaving less ITZ at the edge of the mold. In order to facilitate subsequent characterization, the edges of the film were removed, leading to the observed difference in drug loading between the two formulations.

3.5.9. In Vitro Drug Release of the ITZ-Loaded Films

As ITZ is a weak base and only ionized at very low pH condition (pH = 3), it is necessary to select an appropriate release medium that enhances the saturated solubility to achieve sink conditions.^[53] In Table 3, ITZ shows a relatively higher saturation solubility in 1% w/v SDS + 0.1 mol L⁻¹ HCl compared with other release mediums. The in vitro release profiles of NCs-loaded film and PM-loaded film are presented in Figure 9, reporting that the overall cumulative drug release of ITZ was improved from NCs formulation compared to that from coarse formulation within 24 h. At this endpoint, $96.76 \pm 9.07\%$ ($2.52 \pm 0.24 \text{ mg}$) of ITZ was released from the NCs-loaded films. Conversely, $72.46 \pm 3.9\%$ ($1.88 \pm 0.10 \text{ mg}$) cumulative drug release of ITZ was obtained from PM-loaded films. Although no significant difference was found in the final cumulative drug release within two formulations, this profile indicated the dissolution rate of the drug from NCs-loaded films was enhanced. According to the

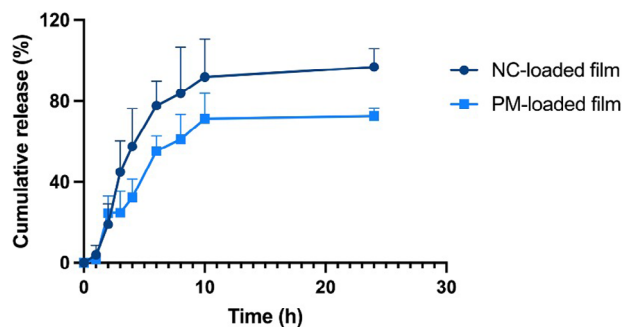


Figure 9. In vitro drug release of ITZ from ITZ-loaded films (means + S.D., $n = 3$).

Noyes-Whitney equation, the increase in dissolution velocity and saturated solubility of solute result from the increased surface area to volume ratio.^[54] Additionally, the Prandtl equation suggests that reducing particle size decreases the diffusional distance, further enhancing the dissolution velocity. Therefore, the simultaneous increase in saturation solubility and the decrease in diffusional distance lead to an overall improved ITZ dissolution.^[55] It was worth noting that the selected release medium was not comparable to the biological conditions in vivo. The release of ITZ from buccal CHI films in buccal environment may involve several steps that ensure effective delivery. Although the fluid on the oral mucosa is limited, there is still enough moisture for diffusion to occur. The ITZ NCs within the CHI matrix can diffuse out of the film and into the surrounding mucosal tissue. In addition, the film may undergo swelling and saliva erosion upon contact with the fluid on the mucosa, thereby facilitating the gradual release of the entrapped ITZ NCs. Furthermore, the inherent mucoadhesive properties of CHI enable the films to adhere to the oral mucosa, prolonging their contact time and facilitating sustained drug release. Therefore, this experiment aimed to establish a controlled model to investigate the difference in dissolution rates between different formulations rather than simulating in vivo conditions.

3.5.10. Buccal Mucosal Deposition of the ITZ-Loaded Films

The mucosal deposition of ITZ from NCs-loaded films and PM-loaded films is depicted in Figure 10A. ITZ NCs films were able to deposit $1360.23 \pm 718.73 \mu\text{g cm}^{-2}$ of drug, whereas a significantly lower deposition was obtained from the PM-loaded films ($58.83 \pm 37.45 \mu\text{g cm}^{-2}$) ($p < 0.05$). The noticeable difference in drug deposition between the two groups could be attributed to the decreased particle size of ITZ, suggesting the improved permeation and penetration ability of ITZ NCs. Another key feature of drug NCs is their enhanced bioadhesiveness compared to coarse microparticles. This improved adhesion is due to the increased number of contact points with biological surfaces, which allows for stronger and more extensive interaction, potentially leading to a higher amount of drug deposition.^[56] Furthermore, the presence of CH around the surface of the NCs may further contribute to their adhesion properties. These inherent bioadhesive properties enhances the ability of NCs to adhere to mucosal tissues, thereby improving drug retention and absorption, which aligns with similar results found in the literature.^[28,57] Noteworthy,

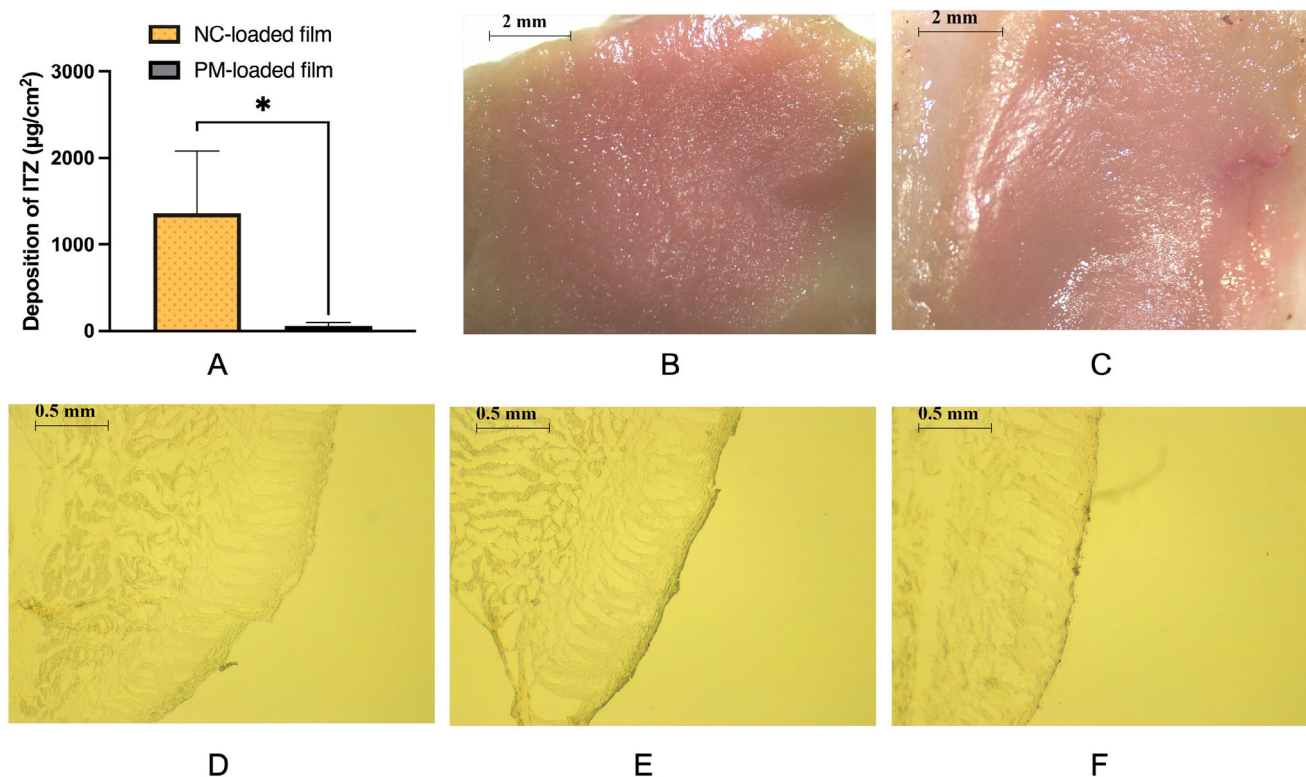


Figure 10. The deposition of ITZ in neonatal porcine oral mucosa A) (means + S.D., $n = 3$); digital microscope images of neonatal porcine oral mucosa after application of NR NCs-loaded film B) and PM-loaded film C); digital microscope images of cross-section of blank neonatal porcine oral mucosa D); digital microscope images of cross-section of neonatal porcine oral mucosa after application of NR NCs-loaded film E) and NR PM-loaded film F).

the high dispersion of the data observed in this study was related to the complex physiology and variability of mucosal tissues, level of hydration, and inter-individual variability, among other factors. Nonetheless, the use of porcine mucosa has proven to be an effective ex vivo model for the assessment of mucosal formulations. To visualize the deposition of NCs, a model dye NR NCs were fabricated and loaded into CHI-based films. Particle size, PDI and zeta potential of NR NCs are exhibited in Section S2, Supporting Information). Figure 10B,C demonstrate that the staining on mucosal surface from NR PM-loaded film was lighter than that from the NR NCs-loaded films. The cross-sections of mucosa applied with different NR NCs-loaded films are shown below. Compared with blank mucosa (Figure 10D), dark staining was observed in mucosa applied with NR NCs-loaded film (Figure 10E), revealing a quicker dissolution and diffusion of the NR NCs into mucosal tissue. However, as presented in Figure 10F, minimal staining was obtained on the mucosal tissue treated with PM-loaded films, indicating limited penetration of NR due to the large particle size. This obvious difference in staining further reinforces the results from the ITZ mucosal deposition.

4. Conclusion

In this work, ITZ NCs with positive or negative charges were successfully prepared using a top-down method with a particle ≈ 200 nm. Cationic NCs exhibited a higher affinity to the negatively charged mucin nanoparticles compared with anionic NCs.

The CHI films containing cationic NCs were fabricated with suitable mechanical properties and homogeneous drug distribution. According to ex vivo mucosal deposition study, a significantly higher amount of drug was delivered to the tissue from NCs-loaded films compared with films containing PM formulation only. This drug delivery platform could potentially enhance the penetration of drug to mucus layer and prolong the residence of the active compounds at the application site for absorption. Besides applications in oral tissues, i.e., treatment of oral candidiasis, this approach may hold potential for addressing fungal infections in other mucosal surfaces, including the vagina. Additionally, due to the flexible texture of the films, they can be easily manipulated for convenient administration and customized individual patient needs. Furthermore, the versatility of mucosal delivery systems enables the incorporation of antifungal agents with other therapeutic agents, such as anti-inflammatory drugs, which may improve treatment outcomes and patient compliance. Overall, this platform holds the promise of improving the penetration of ITZ to buccal mucosa. Crucially, in the future, the antifungal performance of the formulation should be evaluated under specific conditions that mimic a fungal infection.

Supporting Information

Supporting Information is available from the Wiley Online Library or from the author.

Acknowledgements

This work was supported by the Royal Society (grant RGS\R1\231342), the Engineering and Physical Sciences Research Council (grant EP/Y001486/1) and a New Lecturer Grant from Applied Microbiology International.

Conflict of Interest

The authors declare no conflict of interest.

Data Availability Statement

The data that support the findings of this study are available from the corresponding author upon reasonable request.

Keywords

buccal film, chitosan, itraconazole, media milling, mucin, nanosuspensions

Received: May 15, 2024

Revised: August 7, 2024

Published online:

- [1] B. M. Boddupalli, Z. N. K. Mohammed, R. Nath A, D. Banji, *J. Adv. Pharm. Technol. Res.* **2010**, *1*, 381.
- [2] S. Jacob, A. B. Nair, S. H. S. Boddu, B. Gorain, N. Sreeharsha, J. Shah, *Pharmaceutics* **2021**, *13*, 1206.
- [3] S. Rossi, G. Sandri, C. M. Caramella, *Drug Discov. Today Technol.* **2005**, *2*, 59.
- [4] J. P. Martins, H. A. Santos, in *Nanotechnology for Oral Drug Delivery: From Concept to Applications*, Elsevier, Cambridge, MA **2020**.
- [5] M. Collado-González, Y. G. Espinosa, F. M. Goycoolea, *Biomimetics* **2019**, *4*, 32.
- [6] L. W. Hsu, P. L. Lee, C. T. Chen, F. L. Mi, J. H. Juang, S. M. Hwang, Y. C. Ho, H. W. Sung, *Biomaterials* **2012**, *33*, 6254.
- [7] N. Bhattarai, J. Gunn, M. Zhang, *Adv. Drug Delivery Rev.* **2010**, *62*, 83.
- [8] M. M. Canali, L. P. Pedrotti, J. Balsinde, C. Ibarra, S. G. Correa, *Eur. J. Pharm. Biopharm.* **2012**, *80*, 418.
- [9] I. Bravo-Osuna, C. Vauthier, H. Chacun, G. Ponchel, *Eur. J. Pharm. Biopharm.* **2008**, *69*, 436.
- [10] M. A. Mohammed, J. T. M. Syeda, K. M. Wasan, E. K. Wasan, *Pharmaceutics* **2017**, *9*, 1.
- [11] L. Peltonen, J. Hirvonen, *Int. J. Pharm.* **2018**, *537*, 73.
- [12] R. H. Müller, S. Gohla, C. M. Keck, *Eur. J. Pharm. Biopharm.* **2011**, *78*, 1.
- [13] P. H. L. Tran, W. Duan, T. T. D. Tran, *Int. J. Pharm.* **2019**, *571*, 118697.
- [14] R. Al-Kassas, M. Bansal, J. Shaw, *J. Controlled Release* **2017**, *260*, 202.
- [15] M. Nakarani, A. Misra, J. Patel, S. Vaghani, *Daru J. Pharmaceut. Sci.* **2010**, *18*, 84.
- [16] A. A. Date, V. B. Patravale, *Curr. Opin. Colloid Interface Sci.* **2004**, *9*, 222.
- [17] E. Roblegg, E. Fröhlich, C. Meindl, B. Teubl, M. Zaversky, A. Zimmer, *Nanotoxicology* **2012**, *6*, 399.
- [18] S. Mouftah, M. M. A. Abdel-Mottaleb, A. Lamprecht, *Int. J. Pharm.* **2016**, *515*, 565.
- [19] F. Cui, C. He, L. Yin, F. Qian, M. He, C. Tang, C. Yin, *Biomacromolecules* **2007**, *8*, 2845.
- [20] C. Giovino, I. Ayensu, J. Tetteh, J. S. Boateng, *Colloids Surf. B Biointerfaces* **2013**, *112*, 9.
- [21] G. Germini, L. Peltonen, *Molecules* **2021**, *26*, 3941.
- [22] J. O. Morales, R. Su, J. T. McConville, *AAPS PharmSciTech* **2013**, *14*, 475.
- [23] J. O. Morales, S. Huang, R. O. Williams, J. T. McConville, *Colloids Surf B Biointerfaces* **2014**, *122*, 38.
- [24] C. Zhang, L. K. Vora, I. A. Tekko, F. Volpe-Zanutto, K. Peng, A. J. Paredes, H. O. McCarthy, R. F. Donnelly, *Int. J. Pharm.* **2023**, *642*, 123108.
- [25] H. Takeuchi, J. Thongborisute, Y. Matsui, H. Sugihara, H. Yamamoto, Y. Kawashima, *Adv. Drug Deliv Rev.* **2005**, *57*, 1583.
- [26] S. Suryani, A. Y. Chaerunisaa, I. M. Joni, R. Ruslin, L. O. A. N. Ramadhan, Y. W. Wardhana, S. H. Sabarwati, *Polymers* **2022**, *14*, 3417.
- [27] G. P. Andrews, L. Donnelly, D. S. Jones, R. M. Curran, R. J. Morrow, A. D. Woolfson, R. K. Malcolm, *Biomacromolecules* **2009**, *10*, 2427.
- [28] M. B. Bianchi, C. Zhang, E. Catlin, G. Sandri, M. Calderón, E. Larrañeta, R. F. Donnelly, M. L. Picchio, A. J. Paredes, *Mater. Today Bio.* **2022**, *17*, 100471.
- [29] Q2(R1) Validation of analytical procedures: text and methodology guidance for industry **2005**, <https://www.fda.gov/vaccines-blood-biologics/guidance-compliance-regulatory-information-biologics/biologics-guidances> (accessed: May 2024).
- [30] J. Li, Z. Wang, H. Zhang, J. Gao, A. Zheng, *Drug Deliv.* **2021**, *28*, 19.
- [31] G. Kapadnis, A. Dey, P. Dandekar, R. Jain, *Polym. Int.* **2019**, *68*, 1054.
- [32] M. T. A. Abbate, I. K. Ramöller, A. H. Sabri, A. J. Paredes, A. J. Hutton, P. E. McKenna, K. Peng, J. A. Hollett, H. O. McCarthy, R. F. Donnelly, *Int. J. Pharm.* **2023**, *640*, 123005.
- [33] S. M. Bashir, G. Ahmed Rather, A. Patrício, Z. Haq, A. A. Sheikh, M. Z. ul H Shah, H. Singh, A. A. Khan, S. Imtiyaz, S. B. Ahmad, S. Nabi, R. Rakhshan, S. Hassan, P. Fonte, *Materials* **2022**, *15*, 1.
- [34] A. M. Cerdeira, M. Mazzotti, B. Gander, *Int. J. Pharm.* **2013**, *443*, 209.
- [35] H. Tanaka, Y. Ochii, Y. Moroto, D. Hirata, T. Ibaraki, K. I. Ogawara, *Pharmaceutics* **2022**, *14*, 2633.
- [36] L. Peltonen, *Pharmaceutics* **2018**, *10*, 104.
- [37] C. Knieke, M. Sommer, W. Peukert, *Powder Technol.* **2009**, *195*, 25.
- [38] P. W. Voorhees, *J. Stat. Phys.* **1985**, *38*, 231.
- [39] P. Leroy, N. Devau, A. Revil, M. Bizi, *J. Colloid Interface Sci.* **2013**, *410*, 81.
- [40] K. B. Sutradhar, S. Khatun, I. P. Luna, *J. Nanotechnol.* **2013**, *2013*, 1.
- [41] R. F. Donnelly, M. J. Garland, D. I. J. Morrow, K. Migalska, T. R. R. Singh, R. Majithiya, A. D. Woolfson, *J. Control Release* **2010**, *147*, 333.
- [42] G. Tejada, N. L. Calvo, M. Morri, M. Sortino, C. Lamas, V. A. Álvarez, D. Leonardi, *Materials* **2023**, *16*, 3586.
- [43] C. L. Jackson, G. B. McKenna, *J. Chem. Phys.* **1990**, *93*, 9002.
- [44] S. Acosta-Ferreira, O. S. Castillo, J. T. Madera-Santana, D. A. Mendoza-García, C. A. Núñez-Colín, C. Grijalva-Verdugo, A. G. Villalderma, A. T. Morales-Vargas, J. R. Rodríguez-Núñez, *Biotechnol. Rep.* **2020**, *28*, e00554.
- [45] C. Muñoz-Núñez, R. Cuervo-Rodríguez, C. Echeverría, M. Fernández-García, A. Muñoz-Bonilla, *Carbohydr. Polym.* **2023**, *302*, 120438.
- [46] E. Szymańska, K. Winnicka, *Mar Drugs* **2015**, *13*, 1819.
- [47] G. M. El Maghraby, A. H. Alomrani, G. M. El Maghraby, A. H. Alomrani, *Sci. Pharm.* **2009**, *77*, 401.
- [48] S. Bates, G. Zografí, D. Engers, K. Morris, K. Crowley, A. Newman, *Pharm. Res.* **2006**, *23*, 2333.
- [49] E. Utomo, J. Domínguez-Robles, Q. K. Anjani, C. J. Picco, A. Korelidou, E. Magee, R. F. Donnelly, E. Larrañeta, *Int. J. Pharm.* **2023**, *5*, 100142.
- [50] A. B. Nair, R. Kumria, S. Harsha, M. Attimarad, B. E. Al-Dhubiab, I. A. Alhaider, *J. Controlled Release* **2013**, *166*, 10.
- [51] F. Ahmadi, Z. Oveisi, M. Samani, Z. Amoozgar, *Res Pharm. Sci.* **2015**, *10*, 1.
- [52] C. Gao, *Appl. Phys. Lett.* **1997**, *71*, 1801.
- [53] J. M. Poirier, G. Cheymol, *Clin. Pharmacokinet.* **1998**, *35*, 461.

- [54] A. A. Noyes, W. R. Whitney, *J. Am. Chem. Soc.* **1897**, 19, 930.
- [55] R. Mauludin, R. H. Müller, C. M. Keck, *Int. J. Pharm.* **2009**, 370, 202.
- [56] M. B. McGuckin, J. Wang, R. Ghanma, N. Qin, S. D. Palma, R. F. Donnelly, A. J. Paredes, *J. Controlled Release* **2022**, 345, 334.
- [57] C. Zhang, S. A. Jahan, J. Zhang, M. B. Bianchi, F. Volpe-Zanutto, S. M. Baviskar, A. Rodriguez-Abetxuko, D. Mishra, E. Magee, B. F. Gilmore, T. R. R. Singh, R. F. Donnelly, E. Larrañeta, A. J. Paredes, *Int. J. Pharm.* **2023**, 648, 123585.